Sex, aggression and pair-bond : a study on the serotonergic regulation of female sexual function in the marmoset monkey

Aubert, Yves

CHAPTER 4

Positron emission tomography assessment of 8-OH-DPAT-mediated changes in an index of cerebral glucose metabolism in female marmosets

Alexander K. Converse[1], Yves Aubert[2,7], Mohammed Farhoud[3], Jamey P. Weichert[3], Ian J. Rowland[4], Nicole M. Ingrisano[5], Kelly A. Allers[6], Bernd Sommer[6] and David H. Abbott[2,5]

[1]Waisman Center, University of Wisconsin-Madison, Madison, WI, USA; [2]Wisconsin National Primate Research Center, University of Wisconsin-Madison, Madison, WI, USA; [3]Department of Radiology, University of Wisconsin-Madison, Madison, WI, USA; [4]Department of Medical Physics, University of Wisconsin-Madison, Madison, WI, USA; [5]Department of Ob/Gyn, University of Wisconsin-Madison, Madison, WI, USA; [6]Department of CNS Diseases, Boehringer Ingelheim, Biberach, Germany; [7]Division of Medical Pharmacology, Leiden/Amsterdam Center for Drug Research, Leiden University Medical Centre, Leiden, The Netherlands

Neuroimage 2012 Mar; 60(1):447-455

ABSTRACT

As part of a larger experiment investigating serotonergic regulation of female marmoset sexual behavior, this study was designed to (1) advance methods for PET imaging of common marmoset monkey brain, (2) measure normalized FDG uptake as an index of local cerebral metabolic rates for glucose, and (3) study changes induced in this index of cerebral glucose metabolism by chronic treatment of female marmosets with a serotonin 1A receptor (5-HT_{1A}) agonist. We hypothesized that chronic treatment with the 5-HT1A agonist 8-OH-DPAT would alter the glucose metabolism index in dorsal raphé (DR), medial prefrontal cortex (mPFC), medial preoptic area of hypothalamus (mPOA), ventromedial nucleus of hypothalamus (VMH), and field CA1 of hippocampus.

Eight adult ovariectomized female common marmosets *(Callithrix jacchus)* were studied with and without estradiol replacement. In a crossover design, each subject was treated daily with 8-OH-DPAT (0.1 mg/kg SC daily) or saline. After 42–49 days of treatment, the glucose metabolism radiotracer FDG was administered to each female immediately prior to 30 min of interaction with her male pairmate, after which the subject was anesthetized and imaged by PET. Whole brain normalized PET images were analyzed with anatomically defined regions of interest (ROI). Whole brain voxelwisemappingwas also used to explore treatment effects and correlations between alterations in the glucose metabolism index and pairmate interactions.

The rank order of normalized FDG uptake was VMH/mPOA>DR>mPFC/CA1 in both conditions. 8-OH-DPAT did not induce alterations in the glucose metabolism index in ROIs. Voxelwise mapping showed a significant reduction in normalized FDG uptake in response to 8-OH-DPAT in a cluster in medial occipital cortex as well as a significant correlation between increased rejection of mount attempts and reduced normalized FDG uptake in an overlapping cluster.

In conclusion, PET imaging has been used to measure FDG uptake relative to whole brain in marmoset monkeys. Voxelwise mapping shows that 8-OH-DPAT reduces this index of glucose metabolism in medial occipital cortex, consistent with alterations in female sexual behavior.

INTRODUCTION

This is a study of the effects of chronic serotonergic manipulation in a nonhuman primate model of female sexual behavior (Barnett et al., 2006). This work applied positron emission tomography (PET) to marmoset brain imaging. The goals of this work involved methods development, determination of cerebral glucose metabolic indices, and measurement of the effect of chronic treatment with a serotonin 1A (5-HT_{1A}) receptor agonist on brain regions implicated in female sexual interactions with a male pairmate.

5-HT is thought to play a central inhibitory role in regulating female sexual behavior by modulating satiety and balancing excitatory neuromodulators (Pfaus, 2009). In this marmoset study, the prototypical 5-HT_{1A} receptor agonist *R*-(+)-8-hydroxy-2-(di-n-propylamino)-tetralin (8-OH-DPAT) was used (Hjorth et al., 1982). In rats, 8-OH-DPAT acutely diminishes female sexual receptivity (Uphouse et al., 1991). Administration of 8-OH-DPAT (1 mg/kg IV) to male rats acutely alters glucose metabolism in a number of brain regions, including decreases in hippocampal areas and increases in motor regions, consistent with the “5-HT behavioral syndrome” (Kelly et al., 1988). Therapeutic efficacy of serotonergic treatments typically requires at least 2 weeks of administration perhaps due to adaptive changes, and therefore it is important to study the chronic effects of pharmacological treatment (Blier and de Montigny, 1994; Blier et al., 1987; Hensler, 2003). The effect of chronic 8-OH-DPAT administration on cerebral glucose metabolism in primates, including humans, has not been reported.

The current study’s focus on PET imaging of female marmoset neural responses to the 5-HT_{1A} agonist 8-OH-DPAT, during male–female pair tests, arises from our interest in understanding the role of 5-HT in regulating female sexual behavior. An estimated 10% of women (Clayton, 2010) show marked distress and interpersonal difficulty because of unwanted, persistent or recurrent low sexual desire (hypoactive sexual desire disorder, HSDD (American Psychiatric Association, 2000)). Psychopathogenesis of HSDD, however, is not known, but neurotransmitter dysfunction has been proposed involving the excitatory regulators dopamine (DA) and norepinephrine (NE), as well as inhibitory 5-HT (Clayton and Hamilton, 2010; Pfaus, 2009). Pharmacological manipulation of 5-HT commonly results in diminished female sexual satisfaction and activity, particularly in women prescribed selective serotonin reuptake inhibitors (SSRIs) for depression (Clayton and Montejo, 2006; Clayton et al., 2002; Patterson, 1993; Rosen et al., 1999; Segraves, 1998). Animal studies that apply 5-HT receptor subtype specific ligands permit mechanistic examination of 5-HT-mediated effects on sexual behavior. There are 7 known 5-HT receptor families, each with its own specific brain

distribution, as well as effects on behavior and physiology (Barnes and Sharp, 1999). We focused on 5-HT_{1A} receptor activation in this study to explore 5-HT involvement in female sexual inhibition, since the sexually receptive female lordosis posture in rats is inhibited by 5-HT_{1A} receptor activation (Ahlenius et al., 1986; Hebert et al., 1995; Uphouse et al., 1992).

Female marmoset monkeys present an opportunity to explore the sexually inhibitory properties of 8-OH-DPAT in a nonhuman primate model that readily translates to humans, as marmosets form stable, long-term, male–female relationships (Abbott et al., 2003) and display modest amounts of sexual behavior (Barnett et al., 2006). Unlike the multiple-mating social structures of rats and many nonhuman primates, such as macaques and baboons, marmoset sexual behavior most commonly occurs within stable male–female pairs (Abbott et al., 2003; Evans and Poole, 1984; Saltzman et al., 2009). By acceptance or rejection of a pairmate's sexual advances, female marmosets can readily promote, prevent or terminate sexual interactions (Kendrick and Dixson, 1986; Stevenson and Poole, 1976), and our recent development of a standardized behavioral testing paradigm permits repeatable, quantitative exploration of neurally active compounds that enhance or diminish female marmoset sexual behavior (Barnett et al., 2006).

Neuroimaging has furthered mechanistic understanding of neural regulation of sexual behavior in both humans and animals (Arnow et al., 2009; Rilling et al., 2004). Recent improvements in PET spatial resolution now permit its application to marmoset brain imaging (Haneda et al., 2007). PET permits longitudinal measures of brain physiology that may be used to study individual differences in treatment response. In the current protocol, pair-bonded female marmosets are observed upon reunion with their male pairmates following a 90-minute separation (Barnett et al., 2006). Measures were performed on the same individuals during chronic 8-OH-DPAT treatment as well as in a control saline treatment condition. To index glucose metabolism during behavioral interactions, we used the trapped tracer [^{18}F]fluorodeoxyglucose (FDG) (Sokoloff et al., 1977). In this protocol, the rate of glucose metabolism during awake, freely moving behavior is reflected by subsequent imaging performed under anesthesia in the PET scanner (Rilling et al., 2001; Tashiro et al., 2001). We identified anatomical location within the marmoset brain using template regions of interest (ROIs) similar to previous methods employed in studies of humans and rats (Lancaster et al., 2007; Rubins et al., 2003). Because template methods may be subject to error due to individual differences in anatomy not accounted for by the coregistration technique, we verified template ROI against individual ROI results.

The goals of this study were to (1) advance methods for PET imaging of

common marmoset monkey brain, (2) measure normalized FDG uptake as an index of local cerebral metabolic rates for glucose, and (3) study changes induced in this index of cerebral glucose metabolism by chronic treatment of female marmosets with a 5-HT_{1A} agonist. We hypothesized that chronic treatment with the 5-HT_{1A} agonist 8-OH-DPAT would yield altered glucose metabolism in the following five ROIs known to have high 5-HT_{1A} density (Moller et al., 2007; Pazos et al., 1987) or to be involved in female proceptive or receptive sexual behavior (Pfaus, 2009): (1) dorsal raphé (DR), containing 5-HT neurons with extensive projections to hypothalamic, limbic, hippocampal and cortical sites, and neurotransmission regulating 5-HT_{1A} receptors (Kakeyama and Yamanouchi, 1996); (2) medial prefrontal cortex (mPFC), involved in executive and inhibitory regulation of behavior, with sexual behavior-relevant contributions from ventral tegmental area dopaminergic projections engaged in responses to sexual and incentive stimuli (Afonso et al., 2007); (3) medial preoptic area of the hypothalamus (mPOA), intimately involved in female proceptive sexual behavior (Dixson and Lloyd, 1988; Graham and Pfaus, 2010; Kendrick and Dixson, 1986), (4) ventromedial nucleus of the hypothalamus (VMH), regulating female sexual receptivity (Dixson and Lloyd, 1988; Griffin and Flanagan-Cato, 2011; Kendrick and Dixson, 1986), and (5) field CA1 of the hippocampus, involved in sexually relevant memory processes (van Wingen et al., 2008).

MATERIALS AND METHODS

Subjects

Female common marmosets were studied (*Callithrix jacchus*, n=8, 425±47 g, age 4.5±0.6 years, mean±standard deviation). Subjects were pair housed with male pairmates at the Wisconsin National Primate Research Center (WNPRC) for 8–20 months before and throughout the duration of the study with lights on during 06:30–18:30 h, as previously described (Barnett et al., 2006). Ovaries were removed and subcutaneous silastic capsules implanted to provide estradiol replacement in 4 of the subjects (serum estradiol during study weeks: 396±184 pg/mL, mid-follicular phase estradiol levels (Barnett et al., 2006)), while the remaining 4 subjects received empty capsules (serum estradiol 68±31 pg/mL, typical of ovariectomized female marmosets (Barnett et al., 2006)). This study was conducted in accordance with the recommendations of the Guide for the Care and Use of Laboratory Animals and the Animal Welfare Act and its subsequent amendments. All animal procedures were reviewed and approved by the Graduate School Animal Care and Use Committee of the University of Wisconsin-Madison. WNPRC, as part

of the University of Wisconsin-Madison Graduate School, is accredited by the Association for Assessment and Accreditation of Laboratory Animal Care.

Experimental protocol

A counterbalanced, cross-over study, that applied within-subject comparisons, was designed to examine the effects of chronic (15–16 weeks) daily (12:00 h–14:00 h) administration of 8-OHDPAT (0.1 mg/kg in 0.4 mL/kg saline, injected subcutaneously (SC); Sigma-Aldrich St. Louis, MO, USA), or 0.4 mL saline SC, with an intervening 6-week washout period.

Behavioral observations of sexual behavior

In order to stimulate sexual interactions upon reunion (Barnett et al., 2006), females and males were separated for 90 min prior to each of four 30-min behavioral tests at 07:00 h–13:00 h (16–24 h after daily administration of 8-OH-DPAT/saline), 5–6 weeks after treatment onset. At the start of each behavioral test, the male was introduced to the female by remote door operation and behavior was manually and digitally recorded by two observers from behind a one-way window (Barnett et al., 2006). Behavioral tests were reanalyzed from the digitally stored recordings in a random fashion by two observers, blinded with respect to treatment.

Brain imaging

Subjects were scanned with FDG PET at 42–49 days following start of treatment with either 8-OH-DPAT or saline. On the day of the PET scan, each female subject was removed from her home cage, placed alone in a test cage for 90 min, injected in the femoral vein with 31.1±6.4 MBq FDG (IBA Romeoville), reunited with her mate after 5.4±1.3 min in a behavioral test cage, and observed for 30 min during pair behavior, as described for behavioral observations above. The subject was then transported to the PET facility, anesthetized with ketamine (10 mg IM), intubated, and maintained on isoflurane (1–3% in O2) for the remaining procedures. Subjects were then positioned in the University ofWisconsin Inveon small animal PET scanner (Siemens, Knoxville), which provides 127 mm axial and 100mm transaxial field of view, 5 μL volumetric resolution, and 6.8% sensitivity (Bao et al., 2009; Constantinescu and Mukherjee, 2009). Subjects were positioned prone and face forward with their heads taped to prevent motion and with their brains located at the center of the field of view. The subjects were warmed with blown air and monitored for heart rate, SpO_2, exhaled CO_2, and rectal temperature. Emission data were acquired for 60 min in list mode with 350–650 keV energy and 3 ns timing windows. Scans started 82.5±6.3 min following FDG injection

and 26.4±5.7 min following ketamine injection. Following the emission scans, a ^{57}Co transmission scan was acquired (120–125 keV).

To obtain anatomical images, each subject was scanned on a separate day under isoflurane anesthesia with the University of Wisconsin small animal 4.7 T MRI (Varian, Palo Alto) using a Varian 72mm ID quadrature coil and a spin echo multi slice sequence (TR=2000 ms, TE=35ms, MA=128×128, FOV=40mm×40mm, slices=40, thickness=1.00 mm, in-plane pixel size=0.31mm×0.31mm).

Brain atlas

A brain atlas of an adult male common marmoset was used to aid anatomical identification (Palazzi and Bordier, 2008). The atlas comprises 48 coronal sections sliced perpendicular to the anterior commissure—posterior commissure line. Uncertainty in the stereotaxic scale due to shrinkage is expected to be within 3% based on comparisons of medial–lateral and anterior–posterior measures of brains before and after freezing. Digital 2D images provided with the atlas were shifted left–right and dorsal–ventral to align the scales between slices (Adobe Illustrator). A slice missing at bregma +0 mm was replaced with a copy of bregma +0.56 mm resulting in 49 slices spaced at 620±45 μmbased on the labeled anteroposterior positions. These 2D images were stacked into a 3D image of 589×584×59 voxels with in-plane pixel sizes of 53.3 μm×53.3 μm and slice thickness of 620.0 μm (ImageJ (Abramoff et al., 2004)).

MR image processing and ROIs

An MR template image was created as follows. The MR image from the first subject scanned (cj1074) was resliced to 0.5 mm cubic voxels and aligned manually (Spamalize, http://brainimaging.waisman.wisc.edu/~oakes) so as to appear symmetric in coronal and axial views and rotated in a sagittal orientation such that the anterior and posterior commissures of the corpus callosum (AC–PC) lay in the same axial plane. A preliminary whole brain mask was drawn on this image. The MR images of the remaining seven subjects were manually coregistered to that of the first subject, and all eight were whole brain normalized and averaged together. Each of the eight images was aligned to this mean image by automated rigid body (6 degrees of freedom, df) coregistration (FSL FLIRT v. 5.5; Oxford Centre for Functional MRI of the Brain) using a normalized mutual information cost function, and whole brain reference and input weights. The resulting eight images were averaged and each was then aligned to this new average by automated affine (9 df) coregistration. The mean of these eight images was taken as the 0.5 mm

cubic voxel MRI template and a whole brain mask was drawn on this template by tracing the inner boundary of the skull, which appears dark in the MRI.

To aid in delineation of ROIs, the 0.5 mm cubic voxel MRI template was resliced and translated manually to match the atlas image, and the same transformation was applied to the individual MRIs. Bilateral ROIs were drawn by two operators on the template and individual MRIs with reference to the atlas for DR, mPFC, mPOA, VMH, and CA1. Inter- and intra-operator comparisons of the drawn ROIs were made by calculating the ratio of the number of overlapping voxels to the average number of voxels between two versions of the same ROI. The second version drawn by the same operator was used for each of the template ROIs. PET scanner resolution effects for each ROI were estimated by smoothing the ROI and its inverse, i.e. Tissue outside the ROI, with a 1.71 mm FWHM Gaussian kernel.

PET image reconstruction

Reconstructions were performed using the scanner vendor's software (Siemens Inveon Acquisition Workplace). Transmission events were sorted into a 2D sinogram (single-slice rebinning, 128 bins, 160 angles, 159 planes) and scaled by a blank sinogram. Emission events were sorted into a single 3D sinogram (128 bins, 160 angles, 159 planes, span 3, ring difference 79, 27 segments, hist.exe v. 2.3.3.8). Images were reconstructed by filtered backprojection with a ramp filter (recon.exe v. 2.222). The resulting images included corrections for accidental coincidences, detector sensitivity, attenuation, and radioactive decay. Consistent with the low scatter fraction expected from the approximately 25 mm diameter marmoset head, scatter correction was found to have a small effect on the whole brain normalized ROI values (e.g. <4% for mPOA), and scatter corrected whole brain normalized radioactivity values were linearly related across subjects to non-corrected values (e.g. r=0.996 for mPOA). Scatter correction was therefore not applied to avoid introducing additional noise. Image dimensions were 128×128×159 with in-plane pixel size 0.776 mm×0.776 mm and slice thickness 0.796 mm.

PET image analysis

Alignment of the PET images to the 0.5 mm cubic voxel MRI template was performed in several steps as follows. The 16 static PET images (n=8 subjects × 2 conditions) were resliced and manually aligned by translations to the MRI template. Each PET image was then automatically aligned to the version of the subject's MRI prior to the final 9 df transformation of that MRI to the template space. This was done with 6 df using a correlation ratio cost function without reference image weighting and then again with weighting

by the template whole brain mask smoothed with a 2 mm Gaussian kernel. For each subject, the 8-OH-DPAT and Saline images were averaged, and the average was aligned by 6 df to the individual MRI. The 8-OH-DPAT and Saline images were again aligned to this aligned average image. As the final alignment step, the 9 df transformation that had been applied to the individual MRI was applied to the 8-OHDPAT and Saline PET images. The PET images were thus aligned within subject and between subject to the 0.5 mm cubic voxel MRI template. The whole brain mask (8601 μL) was trimmed to avoid radioactivity outside the brain by masking it at the edges with a thresholded version of an intermediate mean PET image (8 subjects × 2 conditions, whole brain normalized radioactivity >1.2, trimmed volume 8065 μL). The individual images were then whole brain normalized, i.e. each pixel value was divided by the average value for the individual in the trimmed whole brain mask. Subtraction images, 8-OH-DPAT minus Saline, were then created, and the trimmed whole brain mask was applied to all images.

ROI analysis was performed in the atlas space. All PET images were coregistered to the atlas using the same transformation that had been applied to the 0.5 mm cubic voxel MRI template. The ROIs drawn on the template and individual MRIs were then applied to the PET images. ROI methods were compared by calculating over the eight subjects the root mean square (RMS) differences of PET image values between operators and between individual MRI- and template-based ROIs. As described below in the Results section, template versus individual MRI differences were comparable to inter-operator differences. Use of template ROIs was therefore considered reliable, and template ROI results were used in the subsequent analyses. Paired 2-tailed Student's t tests were performed on the ROI results in the Saline and 8-OH-DPAT conditions. Significance at $p<0.05$ was required for testing the primary hypothesis of a treatment effect in any of the five bilateral ROIs.

Voxelwise whole brain analysis was also performed in the atlas space. To search for a treatment effect, a paired t test was performed between the 8-OH-DPAT and Saline images. To search for correlations between the glucose metabolism index and behavioral response to 8-OH-DPAT (from quantitative observations made during weeks 5–6 described above), a linear regression with zero intercept was performed between the difference images and the behavioral difference scores (8-OH-DPAT minus Saline). In addition, linear regression was performed on the Saline condition images against sexual behavior in the Saline condition. Two-tailed t test or Pearson r thresholds were set corresponding to $p_{uncorrected}<0.05$ at each voxel, and clusters of voxels with significance $p_{corrected}<0.05$ 2-tailed were identified by random field theory (SPM8) (Worsley et al., 1996).

RESULTS

Image alignment and ROIs

As one goal of this study was methods development, we evaluated the image alignment and ROI delineation procedures. In each subject's aligned MRI, visual inspection of the brain contour seen in every coronal slice demonstrated alignment with the mean MRI to within 0.5 mm (Suppl. Fig. 1). The resulting MRI template is shown in Fig. 1. The 16 aligned individual PET images (8 subjects × 2 conditions) agreed to≤0.5 mm between individuals and to higher precision within subjects (Suppl. Fig. 2). There were visible differences between subjects and between conditions in relative FDG uptake in tissue outside the skull, but the trimmed whole brain mask prevented spillover into observed brain regions. Fig. 2 shows the MRI template and mean FDG image

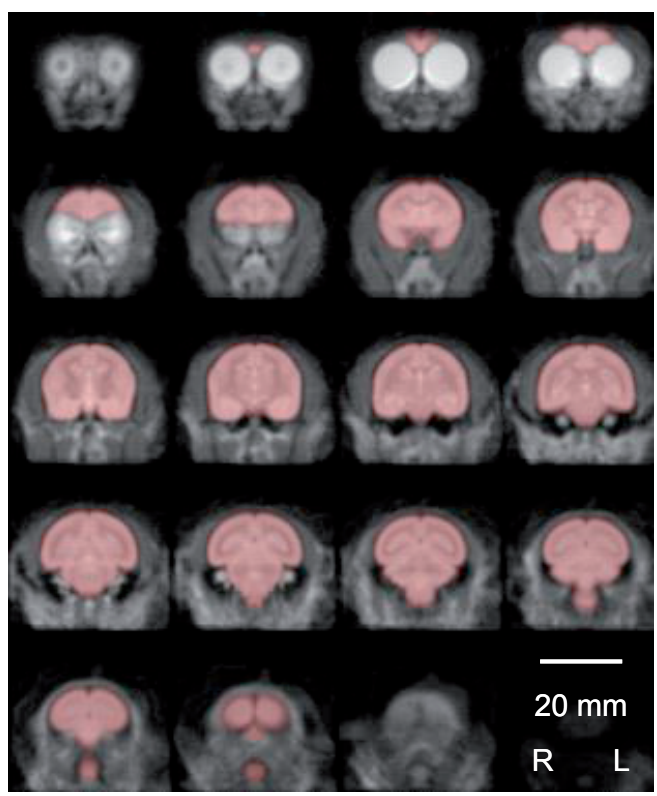

Fig. 1. MRI template. Mean of aligned images (n=8) used as MRI template (Every fourth 0.5 mm coronal slice shown). Whole brain mask is overlaid (red). The template is freely available upon request to the corresponding author.

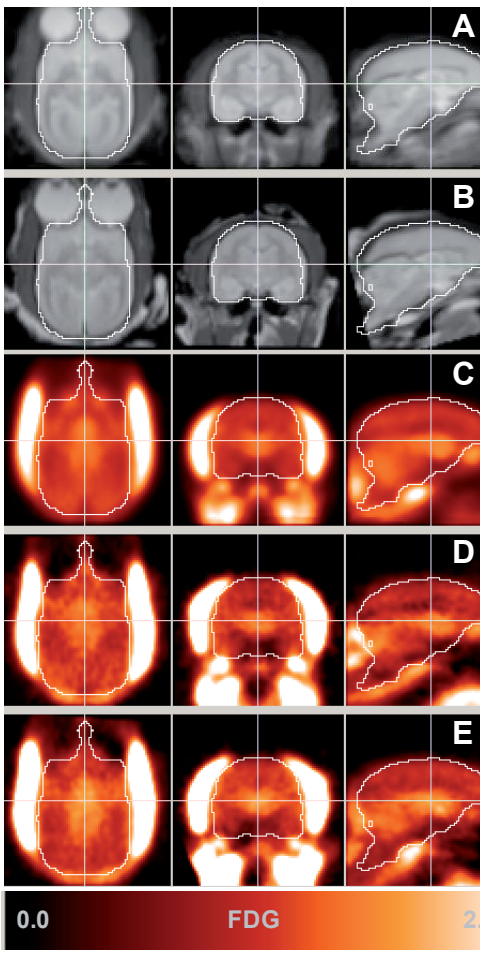

Fig. 2. Aligned images. Axial, coronal, and sagittal slices of MRI template (A, n=8 subjects), MRI of one subject (B, cj1022), mean FDG image (C, n=8 subjects × 2 conditions), and FDG image of one subject (cj1022) in Saline condition D and 8-OH-DPAT condition E. Contour is on whole brain mask trimmed to avoid contributions from radioactivity uptake outside of the brain. Color scale indicates whole brain normalized radioactivity concentration shown in C–E.

(shown in greater detail in Suppl. Fig. 3) along with typical single subject MRI and FDG images in the two conditions. Representative slices of the template MRI aligned to the atlas and the ROIs are shown in Fig. 3.

Methods for delineating ROIs were compared, and resolution effects were estimated. Comparing ROIs delineated on individual MRIs (5 regions × 8 subjects), intra- and inter-operator overlap were 0.86±0.05 (n=40) and 0.85±0.06 (n=40), respectively. Intra- and inter-operator overlap of the five template ROIs were 0.89±0.03 (n=5) and 0.84±0.06 (n=5), respectively. Degrees of differences in FDG values between operators and between methods were highly comparable: 8-OH-DPAT minus Saline values were compared across the eight subjects and the five bilateral ROIs, and the average (n=5) root mean square difference (n=8) was 0.0083±0.0034 for

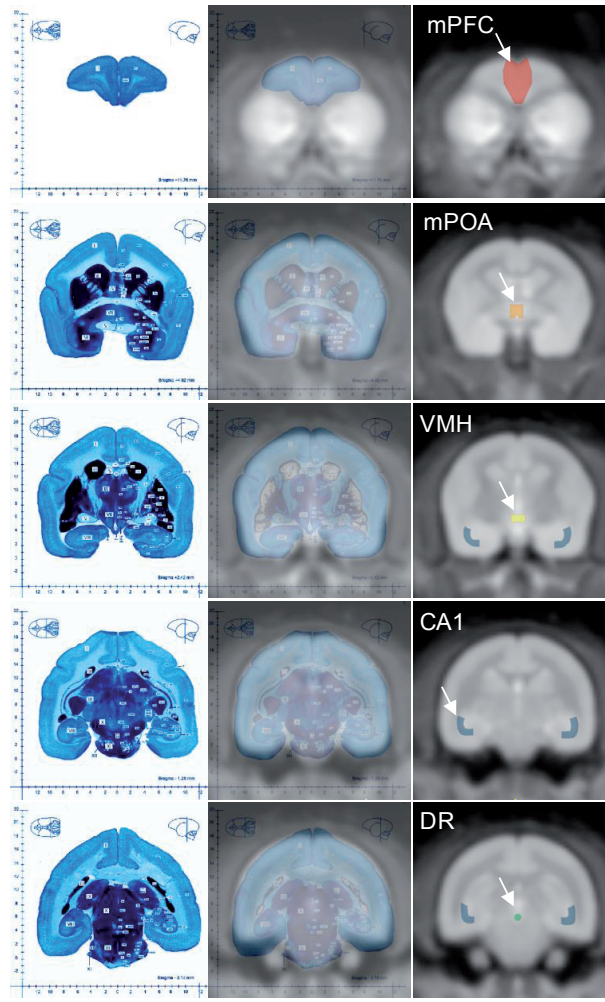

Fig. 3. Anatomical identification. Fusion image (center column) of coregistered brain atlas (left column) and MRI template (right column). Representative coronal slices showing regions of interest (ROIs) for medial prefrontal cortex (mPFC), medial preoptic area of the hypothalamus (mPOA), ventromedial hypothalamic nucleus (VMH), field CA1 of the hippocampus (CA1), and dorsal raphe nucleus (DR). Atlas images courtesy of Springer Science+Business Media (Palazzi and Bordier, 2008).

inter-operator comparisons and 0.0092±0.0034 for individual MRI-determined versus template MRI-determined comparisons. Subsequent analyses were thus performed using only template MRI-determined ROIs. The template ROIs had the following bilateral volumes: DR 1.5 µL, mPFC 100.4 µL, mPOA 4.9 µL, VMH 5.2 µL, and CA1 46.8 µL. Upon simulating the PET scanner resolution (5 µL) with assumed uniform distribution of radioactivity, the activity calculated in the ROI originating in the ROI itself was DR 14%, mPFC 66%, mPOA 29%, VMH 28%, and CA1 36%. No partial volume correction was applied to the measured data, and the reported results must, therefore, be considered best estimates for the delineated ROIs.

Experimental conditions

Experimental conditions for the PET scans are presented in Table 1. There were no significant differences in parameters between treatment conditions. No significant effect of estradiol group was observed in the Saline condition in the ROIs or by voxelwise analysis, nor was there a significant estradiol × 8-OH-DPAT interaction (two way ANOVA with repeated measures). Subsequent results were therefore calculated without reference to estradiol group.

Table 1. Experimental parameters. Mean±SD (n=8), p: paired t test 2-tailed. WB=mean radioactivity concentration in whole brain (MBq/mL), ID=injected dose (MBq), and BW=body weight (g).

	Saline	8-OH-DPAT	p
Age (years)	4.54 ± 0.72	4.54 ± 0.52	1.00
Weight (g)	427 ± 54	422 ± 42	0.44
Injected FDG (MBq)	32.1 ± 7.3	29.9 ± 5.4	0.51
Behavior start–FDG inject (min)	5.4 ± 1.2	5.4 ± 1.5	0.93
Scan start time	11:24 ± 1:09	10:50 ± 1:06	0.15
Scan start–last treatment (h)	22.6 ± 1.3	21.9 ± 1.1	0.14
Scan start–FDG inject (min)	83.1 ± 6.6	82.0 ± 6.3	0.73
Scan start–ketamine inject (min)	27.3 ± 6.5	25.5 ± 5.0	0.50
WB/(ID/BW) (g/mL)	1.06 ± 0.17	0.99 ± 0.13	0.27

Normalized FDG uptake during saline administration and response to treatment

In the Saline as well as the 8-OH-DPAT condition, mean FDG values ranked VMH / mPOA>DR>mPFC / CA1 (Suppl. Fig. 4). Paired t tests indicated no

Table 2. FDG results. Whole brain normalized radioactivity measures in anatomically defined ROIs for Saline condition, 8-OH-DPAT condition, and the difference 8-OH-DPAT minus Saline. (p: paired t test, 2-tailed; n=8).

ROI	V (μL)	Saline	8-OH-DPAT	8-OH-DPAT minus saline	p
DR	1.5	1.164 ± 0.168	1.169 ± 0.113	0.004 ± 0.115	0.922
mPFC	100.4	0.988 ± 0.055	0.981 ± 0.050	−0.007 ± 0.090	0.844
mPOA	4.9	1.292 ± 0.245	1.324 ± 0.249	0.031 ± 0.096	0.387
VMH	5.2	1.349 ± 0.310	1.359 ± 0.232	0.010 ± 0.134	0.832
CA1	46.8	0.987 ± 0.037	0.983 ± 0.045	−0.005 ± 0.042	0.763

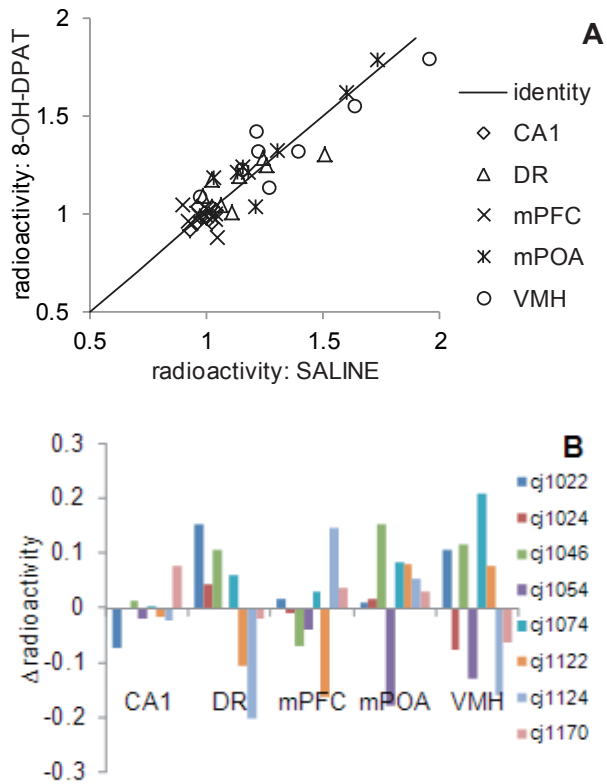

Fig. 4. ROI analysis of response to 8-OH-DPAT treatment. Scatter plot showing individual ROI results (whole brain normalized radioactivity) in 8-OH-DPAT and saline conditions (A). Bar plot shows difference in whole brain normalized radioactivity (8-OH-DPAT minus saline) for each ROI and each subject (B). No ROI shows a significant response to chronic 8-OH-DPAT treatment ($p>0.3$ for each region; paired t test, 2-tailed; n=8).

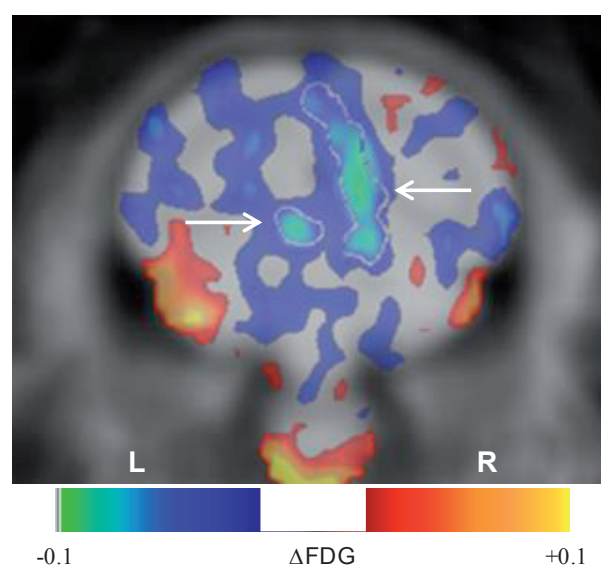

Fig. 5. Glucose metabolism index decreases in medial occipital cortex in response to chronic 8-OH-DPAT treatment. The color scale indicates the mean difference in whole brain normalized radioactivity, ΔFDG = 8-OH-DPAT minus Saline. White contour marked by arrows delineates a significant negative 3D cluster in the corresponding t map, shown at Bregma −11.2 mm (2-tailed paired t test, $p_{uncorrected}<0.05$, extent=60 μL, $p_{corrected}=0.004$). Mean difference arbitrarily thresholded at $0.02<|\Delta FDG|<0.10$.

8-OH-DPAT-induced difference in the magnitude of FDG uptake in any ROI (Table 2 and Fig. 4). Voxelwise mapping of 8-OH-DPAT minus Saline revealed a single cluster in medial occipital cortex of reduced activity (8-OH-DPAT < Saline, $p_{uncorrected}$<0.05, extent=60 µL, $p_{corrected}$=0.004; Fig. 5 and Suppl. Fig. 5).

Behavior

To further confirm the significance of the finding of decreased normalized FDG uptake in medial occipital cortex in response to 8-OHDPAT, we considered alterations in female rejection of male mounts and mount attempts (the most significant 8-OH-DPAT-induced behavioral finding) (Aubert et al., in press). The between-condition difference in FDG uptake was therefore correlated voxelwise against the difference in rejection of mount attempts. Two significant clusters of voxels were found, in which altered normalized FDG uptake correlated with altered rejection of mounts (Fig. 6 and Supp. Fig. 6; $p_{uncorrected}$<0.05; positive correlation: left ventral cerebellum, extent=48 µL, $p_{corrected}$=0.017; negative correlation: medial occipital cortex, extent=72 µL, $p_{corrected}$=0.001). The second cluster, in which decreased metabolism correlated with increased rejection of mounts, overlapped 38% with the cluster of voxels described above that exhibited reduced metabolism during 8-OH-DPAT treatment (Fig. 7 and Suppl. Fig. 7). Subsequent exploration of the relation between normalized FDG uptake and rejection of mount attempts in the Saline condition alone yielded three significant clusters (Table 3, Suppl. Fig. 8), but the mean normalized FDG uptake in these clusters did not reveal a significant response to 8-OH-DPAT (p>0.5, 2-tailed paired t test).

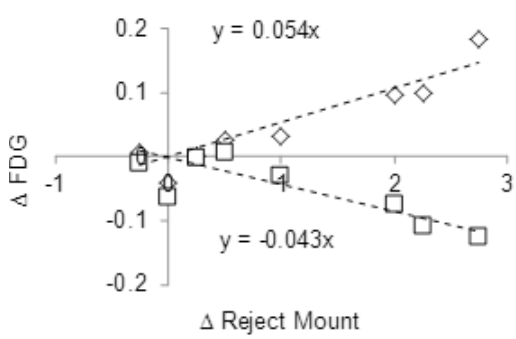

Fig. 6. Rejection of mounts. Between-condition difference in normalized FDG uptake (8-OH-DPAT - Saline) plotted against alteration in behavior for the eight subjects. Voxelwise analysis found two significant clusters (Suppl. Fig. 6), one with a positive correlation (◊ left ventral cerebellum) and one with a negative correlation (□ medial occipital cortex).

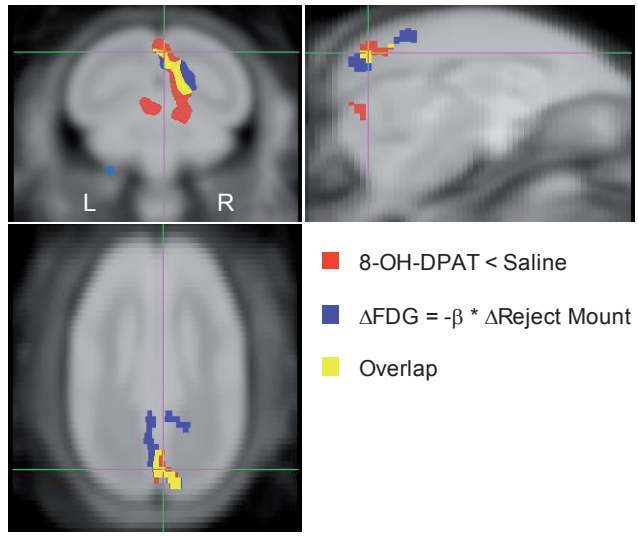

Fig. 7. Glucose metabolism index and behavior respond to 8-OH-DPAT treatment in concert. Orthogonal views of MRI template at medial occipital cortex. Cluster of voxels with significant reduction in FDG radioactivity during 8-OH-DPAT condition compared to Saline condition (red; paired t test, 2-tailed $p_{uncorrected}$<0.05, extent 60 μL, $p_{corrected}$=0.004). Cluster of voxels with significant negative correlation between alterations of FDG radioactivity and rejection of mount attempts between conditions (blue; Pearson r; 2-tailed $p_{uncorrected}$<0.05, extent 72 μL, $p_{corrected}$=0.001). The two clusters overlap (yellow). Part of significant cluster with positive correlation is seen in coronal view (light blue at ventral left edge of cerebellum).

Table 3. Significant clusters identified by voxelwise statistical mapping. Clusters in t maps above threshold at $p_{uncorrected}$=0.05 with extent shown in μL. $p_{corr.}$=p value of cluster corrected for familywise error (SPM8). Position of maximum absolute t value (max. |t|) within cluster indicated in atlas coordinates (mm) (Palazzi and Bordier, 2008): LR=right with respect to midline, AP=anterior w.r.t. bregma, and DV=dorsal w.r.t. interaural line. Atlas origin corresponds to voxel (x,y,z)=(298,30,111).

Test	Region	μL	$p_{corr.}$	max. |t|	LR	AP	DV
Contrast: 8-OH-DPAT minus saline							
	Medial occipital cortex	60	0.004	−14.4	0.6	−11.2	13.5
Correlation: ΔFDG vs Δreject mount							
	Medial occipital cortex	72	0.001	−15.4	1.0	−11.8	12.1
	Left ventral cerebellum	48	0.017	9.7	−4.4	−8.1	0.5
Correlation: FDG vs reject mount (saline)							
	Bilateral ventral cerebellum	161	0.000	11.9	−2.6	−3.7	−1.9
	Bilateral dorsal frontal cortex	115	0.001	16.2	−2.1	5.6	19.0
	Bilateral orbitofrontal cortex	122	0.000	−8.8	8.5	7.4	10.2

DISCUSSION

In this work, we (1) advanced methods for PET imaging of marmoset monkey brain, (2) measured whole brain normalized FDG uptake as an index of local cerebral metabolic rates for glucose, and (3) studied the effect of chronic treatment with a 5-HT1A receptor agonist on brain regions implicated in regulating female sexual interactions.

Anatomical identification

In this work we implemented and validated a novel templatebased method of anatomical identification for PET imaging of marmoset brain. This relied on adequate alignment of the individual MR images to the template space and of PET images to MRIs (Figs. 1 and 2). Alignment of the MRI template to the published histological atlas was within 1 mm, a very satisfactory degree of agreement. While the agreement between the MRI template and the atlas was not sufficient to simply delineate ROIs on the atlas, it aided identification of regions in the MRI by means of relative positions to common features seen in each image (Fig. 3). Despite the excellent alignment between the individual MRIs, as judged by brain contours (Fig. 2), individual anatomical differences in grey-white contrast within the brain may still be significant. Inter-operator variances, however, in geometric overlap and in FDG measures using individual ROIs were comparable to individual- versus template-determined differences. The template ROI method may therefore provide anatomical identification as reproducible as that obtained by delineating regions on individual MRIs. While template ROI location was reliable between subjects, measures attributed to the smaller regions, namely DR, mPOA, and VMH, must be interpreted with caution because of the PET scanner resolution.

Glucose metabolism index and behavior

This is the first report, to our knowledge, of the effect of chronic 8-OH-DPAT administration on cerebral glucose metabolism in primates. Despite relatively large differences in whole brain normalized radioactivity measured between regions and between subjects, FDG measures in the anatomically defined ROIs were generally stable between conditions. Indeed, none of the anatomically defined ROIs exhibited a significant response to 8-OH-DPAT (Table 2 and Fig. 4). On the other hand, voxelwise analysis of 8-OH-DPAT versus Saline identified a significant cluster of reduced metabolism in medial occipital cortex (Fig. 5).

A limitation of this study was the lack of absolute quantification of cerebral glucose metabolism. Because FDG uptake occurred during freely moving behavior, blood sampling would have interfered with the experiment, so

normalized FDG uptake was used as an index of glucose metabolism. The between condition measures reported here therefore only indexed alterations in metabolism relative to whole brain, and interpreting them as changes in absolute glucose metabolism is therefore complicated by potential changes in global cerebral metabolism (Borghammer et al., 2009). The reduction in whole brain normalized radioactivity observed in medial occipital cortex (−5.9%, $p_{corrected}$=0.004) was supported by dimunition of radioactivity in that region normalized to injected dose / body weight (−13.2%, p=0.093, 2-tailed paired t test) suggesting a true reduction in neural activity.

The observed 8-OH-DPAT induced reduction of normalized FDG uptake in medial occipital cortex overlapped 38% with a brain region showing a correlation between 8-OH-DPAT-induced increase in female rejection of male mounts and 8-OH-DPAT-induced reduction in FDG uptake (Figs. 6–7). Such an association between 8-OH-DPAT-induced changes in female sexual behavior and normalized FDG uptake in occipital cortex is perhaps not surprising when considering that primate occipital cortex receives considerable 5-HT innervation (Morrison et al., 1982) associated with processing of visual information involving 5-HT_{1A}, 5-HT_{1B}, and 5-HT_{2A} receptors (Gebhard et al., 1993; Watakabe et al., 2009; Yamamori, 2011).

Our detailed knowledge of within-neuron location of 5-HT receptor subtypes within occiptal cortex derives from rodent studies, in which hyperpolarizing 5-HT_{1A} receptors are found on the soma and axon hillock of layer 5 pyramidal (L5P) neurons (Moreau et al., 2010). L5P neurons, after integrating thalamocortical inputs relayed mostly from L2/3 visual cortex neurons, elaborate cortical outputs from the visual cortex to multiple areas of the cortex (Thomson and Bannister, 1998). Axon hillock 5-HT1A receptors on L5P neurons have been shown to provide crucial inhibitory contributions in balancing excitation and inhibition, possibly by regulating gain control (enhancing weak signals and suppressing excessive responses) (Amargos-Bosch et al., 2004; Moreau et al., 2010; Yamamori, 2011). In this study, therefore, 8-OH-DPAT-mediated chronic overstimulation of axon-hillock 5-HT_{1A} receptors on L5P visual cortical neurons may decrease the likelihood of L5P activity and potentially produce an area-wide overall decrease in glucose metabolism. Such enhanced $5HT_{1A}$-mediated inhibition of female marmoset visual cortex L5P synaptic output may thus distort visually-relevant signals required for timely cortical processing. This disrupted cortical processing could in turn contribute to the 8-OH-DPAT-mediated inhibition of female engagement in sexual behavior with their male pairmates, as the visual cortex projects to, and receives input from, the amygdala (Amaral, 2002) and frontal cortex (Catani et al., 2002; Nieuwenhuys et al., 1988), 5-HT responsive regions that

are intimately involved in attributing salience, and directing visual attention, to negative emotional stimuli (Surguladze et al., 2008).

To identify brain regions associated with female marmoset sexual behavior, we subsequently correlated normalized FDG uptake with female rejection of mounts in the Saline condition alone, which yielded three significant clusters of voxels. A cluster encompassing bilateral orbitofrontal cortex and right insular cortex exhibited increasing FDG uptake across subjects with decreasing female rejection of mounts. This result is consistent with those from human neuroimaging studies, in which women were exposed to erotic visual stimuli (Arnow et al., 2009) or to male faces (Rupp et al., 2009). There was no significant change in FDG uptake observed in any of these three clusters of voxels in response to 8-OH-DPAT. The lack of 8-OH-DPAT related changes in FDG uptake in these voxel clusters suggests that individual differences in these regions are relatively stable and 8-OH-DPAT induced alteration in female mount rejection is mediated by other brain regions, in particular the medial occipital region discussed above.

Taken together, these observations support the notion that the association between 8-OH-DPAT-related changes in behavior and occipital cortex FDG uptake may indicate altered salience of, and visual attention paid to, pairmate interactions contributing to diminished female sexual receptivity. Further planned investigations of the effects of chronic 8-OH-DPAT administration on the primate serotonergic system, particularly upon 5-HT_{1A} and SERT availability, may shed light on this question.

CONCLUSIONS

This work implemented and validated a template method of marmoset brain PET analysis that yielded reliable measures of normalized FDG uptake. Chronic treatment with 8-OH-DPAT (0.1 mg/kg SC daily for 42–49 days) did not produce significant alterations in this glucose metabolism index in the five anatomically defined regions examined (DR, mPFC, mPOA, VMH, and CA1) in awake, behaving, ovariectomized adult female marmosets with or without estradiol replacement. Parametric mapping revealed a significant reduction in the glucose metabolism index in response to 8-OH-DPAT in medial occipital cortex, consistent with alterations in female sexual behavior.

ACKNOWLEDGMENTS

The authors are grateful to the WNPRC veterinary staff including Dr. Kevin G. Brunner and Victoria R. Carter as well as to Amber K. Edwards, Morgan L.

Gustison, and Nicole R. Diol for assistance with ROI delineation.

This study was funded by Boehringer Ingelheim (to DHA). Additional funding for facilities was provided by NIH grants 5P51RR000167-50, RR15459-01, RR020141-01, 2P30CA014520-34, and 1S10RR019194-01A1.

REFERENCES

Abbott, D.H., Barnett, D.K., Colman, R.J., Yamamoto, M.E., Schultz-Darken, N.J., 2003. Aspects of common marmoset basic biology and life history important for biomedical research. Comp. Med. 53 (4), 339–350.

Abramoff,M.D.,Magelhaes, P.J., Ram, S.J., 2004. Image processing with ImageJ. Biophotonics Int. 11, 36–42.

Afonso, V.M., Sison, M., Lovic, V., Fleming, A.S., 2007. Medial prefrontal cortex lesions in the female rat affect sexual and maternal behavior and their sequential organization. Behav. Neurosci. 121 (3), 515–526.

Ahlenius, S., Fernandezguasti, A., Hjorth, S., Larsson, K., 1986. Suppression of lordosis behavior by the putative 5-ht receptor agonist 8-oh-dpat in the rat. Eur. J. Pharmacol. 124 (3), 361–363.

Amaral, D.G., 2002. The primate amygdala and the neurobiology of social behavior: implications for understanding social anxiety. Biol. Psychiatry 51 (1), 11–17.

Amargos-Bosch, M., Bortolozzi, A., Puig, M.V., Serrats, J., Adell, A., Celada, P., Toth, M., Mengod, G., Artigas, F., 2004. Co-expression and in vivo interaction of serotonin (1A) and serotonin (2A) receptors in pyramidal neurons of prefrontal cortex. Cereb. Cortex 14 (3), 281–299.

American Psychiatric Association, 2000. Diagnostic and statistical manual of mental disorders: DSM-IV-TR, 4th edition.

Arnow, B.A., Millheiser, L., Garrett, A., Lake Polan, M., Glover, G.H., Hill, K.R., Lightbody, A., Watson, C., Banner, L., Smart, T., et al., 2009.Womenwith hypoactive sexual desire disorder compared to normal females: a functional magnetic resonance imaging study. Neuroscience 158 (2), 484–502.

Aubert, Y., Gustison, M.L., Gardner, L.A., Bohl, M.A., Lange, J.R., Allers, K.A., Sommer, B., Datson, N.A., Abbott, D.H., in press. Flibanserin and 8-OH-DPAT implicate serotonin in association between female marmoset monkey sexual behavior and changes in pair-bond quality. J. Sex. Med. doi:10.1111/j.1743-6109.2011.02616.x.

Bao, Q., Newport, D., Chen, M., Stout, D.B., Chatziioannou, A.F., 2009. Performance evaluation of the inveon dedicated PET preclinical tomograph based on the NEMA NU-4 standards. J. Nucl. Med. 50 (3), 401–408.

Barnes, N.M., Sharp, T., 1999. A review of central 5-HT receptors and their function. Neuropharmacology 38 (8), 1083–1152.

Barnett, D.K., Bunnell, T.M., Millar, R.P., Abbott, D.H., 2006. Gonadotropin-releasing hormone II stimulates female sexual behavior in marmoset monkeys. Endocrinology 147 (1), 615–623.

Blier, P., de Montigny, C., 1994. Current advances and trends in the treatment of depression. Trends Pharmacol. Sci. 15 (7),

220–226.

Blier, P., de Montigny, C., Chaput, Y., 1987. Modifications of the serotonin system by antidepressant treatments—implications for the therapeutic response in major depression. J. Clin. Psychopharmacol. 7 (6), S24–S35.

Borghammer, P., Cumming, P., Aanerud, J., Foerster, S., Gjedde, A., 2009. Subcortical elevation of metabolism in parkinson's disease—a critical reappraisal in the context of global mean normalization. Neuroimage 47 (4), 1514–1521.

Catani, M., Howard, R.J., Pajevic, S., Jones, D.K., 2002. Virtual in vivo interactive dissection of white matter fasciculi in the human brain. Neuroimage 17 (1), 77–94.

Clayton, A.H., 2010. The pathophysiology of hypoactive sexual desire disorder in women. Int. J. Gynecol. Obstet. 110 (1), 7–11.

Clayton, A.H., Hamilton, D.V., 2010. Female sexual dysfunction. Psychiatr. Clin. North Am. 33 (2), 323–338.

Clayton, A.H., Montejo, A.L., 2006. Major depressive disorder, antidepressants, and sexual dysfunction. J. Clin. Psychiatry 67, 33–37.

Clayton, A., Pradko, J., Croft, H., Montano, C., Leadbetter, R., Bolden-Watson, C., Bass, K., Donahue, R., Jamerson, B., Metz, A., 2002. Prevalence of sexual dysfunction among newer antidepressants. J. Clin. Psychiatry 63 (4), 357–366.

Constantinescu, C.C., Mukherjee, J., 2009. Performance evaluation of an inveon PET preclinical scanner. Phys. Med. Biol. 54 (9), 2885–2899.

Dixson, A.F., Lloyd, S.A.C., 1988. The hormonal and hypothalamic control of primate sexual behaviour. Symp. Zool. Soc. Lond. 60, 81–117.

Evans, S., Poole, T.B., 1984. Long-term changes and maintenance of the pair-bond in common marmosets, callithrix-jacchus-jacchus. Folia Primatol. 42 (1), 33–41.

Gebhard, R., Zilles, K., Schleicher, A., Everitt, B.J., Robbins, T.W., Divac, I., 1993. Distribution of 7 major neurotransmitter receptors in the striate cortex of the new-world monkey callithrix-jacchus. Neuroscience 56 (4), 877–885.

Graham, M.D., Pfaus, J.G., 2010. Differential regulation of female sexual behaviour by dopamine agonists in the medial preoptic area. Pharmacol. Biochem. Behav. 97 (2), 284–292.

Griffin, G.D., Flanagan-Cato, L.M., 2011. Ovarian hormone action in the hypothalamic ventromedial nucleus: remodelling to regulate reproduction. J. Neuroendocrinol. 471.

Haneda, E., Higuchi, M., Maeda, J., Inaji, M., Okauchi, T., Ando, K., Obayashi, S., Nagai, Y., Narazaki, M., Ikehira, H., et al., 2007. In vivo mapping of substance P receptors in brains of laboratory animals by high-resolution imaging systems. Synapse 61 (4), 205–215.

Hebert, T., Menard, C., Dohanich, G., 1995. Inhibition of lordosis in female hamsters and rats by 8-OH-DPAT treatment. Physiol. Behav. 57 (3), 523–527.

Hensler, J.G., 2003. Regulation of 5-HT1A receptor function in brain following agonist or antidepressant administration. Life Sci. 72 (15), 1665–1682.

Hjorth, S., Carlsson, A., Lindberg, P., Sanchez, D., Wikstrom, H., Arvidsson, L.E., Hacksell, U., Nilsson, J.L.G., 1982. 8-hydroxy-2-(di-normal-propylamino)tetralin,

8-oh-dpat, a potent and selective simplified ergot congener with central 5-ht-receptor stimulating activity. J. Neural Transm. 55 (3), 169–188.

Kakeyama, M., Yamanouchi, K., 1996. Inhibitory effect of baclofen on lordosis in female and male rats with dorsal raphe nucleus lesion or septal cut. Neuroendocrinology 63 (3), 290–296.

Kelly, P.A.T., Davis, C.J., Goodwin, G.M., 1988. Differential patterns of local cerebral glucose-utilization in response to 5-Hydroxytryptamine1 agonists. Neuroscience 25 (3), 907–915.

Kendrick, K., Dixson, A., 1986. Anteromedial hypothalamic-lesions block proceptivity but not receptivity in the female common marmoset (callithrix-jacchus). Brain Res. 375 (2), 221–229.

Lancaster, J.L., Tordesillas-Gutierrez, D., Martinez, M., Salinas, F., Evans, A., ZilleS, K., Mazziotta, J.C., Fox, P.T., 2007. Bias between MNI and talairach coordinates analyzed using the ICBM-152 brain template. Hum. Brain Mapp. 28 (11), 1194–1205.

Moller, M., Jakobsen, S., Gjedde, A., 2007. Parametric and regional maps of free serotonin 5HT(1A) receptor sites in human brain as function of age in healthy humans. Neuropsychopharmacology 32 (8), 1707–1714.

Moreau, A.W., Amar, M., Le Roux, N., Morel, N., Fossier, P., 2010. Serotoninergic fine-tuning of the excitation–inhibition balance in rat visual cortical networks. Cereb. Cortex 20 (2), 456–467.

Morrison, J.H., Foote, S.L., Molliver, M.E., Bloom, F.E., Lidov, H.G.W., 1982. Noradrenergic and serotonergic fibers innervate complementary layers in monkey primary visual-cortex—an immunohistochemical study. Proc. Natl. Acad. Sci. U. S. A.-Biol. Sci. 79 (7), 2401–2405.

Nieuwenhuys, R.J., Voogd, J., van Huijzen, C., 1988. The human central nervous system. Springer-Verlag, Berlin.

Palazzi, X., Bordier, N., 2008. The Marmoset Brain in Stereotaxic Coordinates. Springer Science+Business Media, New York.

Patterson, W., 1993. Fluoxetine-induced sexual dysfunction. J. Clin. Psychiatry 54 (2), 71-71.

Pazos, A., Probst, A., Palacios, J., 1987. Serotonin receptors in the human-brain. 3. Autoradiographic mapping of serotonin-1 receptors. Neuroscience 21 (1), 97–122.

Pfaus, J.G., 2009. Pathways of sexual desire. J. Sex. Med. 6 (6), 1506–1533.

Rilling, J.K., Winslow, J.T., O'Brien, D., Gutman, D.A., Hoffman, J.M., Kilts, C.D., 2001. Neural correlates of maternal separation in rhesus monkeys. Biol. Psychiatry 49 (2), 146–157.

Rilling, J.K., Winslow, J.T., Kilts, C.D., 2004. The neural correlates of mate competition in dominant male rhesus macaques. Biol. Psychiatry 56 (5), 364–375.

Rosen, R.C., Lane, R.M., Menza, M., 1999. Effects of SSRIs on sexual function: a critical review. J. Clin. Psychopharmacol. 19 (1), 67–85.

Rubins, D.J., Melega, W.P., Lacan, G., Way, B., Plenevaux, A., Luxen, A., Cherry, S.R., 2003. Development and evaluation of an automated atlas-based image analysis method for microPET studies of the rat brain. Neuroimage 20 (4), 2100–2118.

Rupp, H.A., James, T.W., Ketterson, E.D., Sengelaub, D.R., Janssen, E., Heiman, J.R., 2009. Neural activation in the orbito-

frontal cortex in response to male faces increases during the follicular phase. Horm. Behav. 56 (1), 66–72.

Saltzman, W., Digby, L.J., Abbott, D.H., 2009. Reproductive skew in female common marmosets: what can proximate mechanisms tell us about ultimate causes? Proc. R. Soc. B Biol. Sci. 276 (1656), 389–399.

Segraves, R., 1998. Antidepressant-induced sexual dysfunction. J. Clin. Psychiatry 59, 48–54.

Sokoloff, L., Reivich, M., Kennedy, C., Des Rosiers, M.H., Patlak, C.S., Pettigrew, K.D., Sakurada, O., Shinohara, M., 1977. The [14C]deoxyglucose method for the measurement of local cerebral glucose utilization: theory, procedure, and normal values in the conscious and anesthetized albino rat. J. Neurochem. 28 (5), 897–916.

Stevenson, M.F., Poole, T.B., 1976. Ethogram of common marmoset (Callithrix jacchus jacchus): general behavioral repertoire. Anim. Behav. 24, 428-451.

Surguladze, S.A., Elkin, A., Ecker, C., Kalidindi, S., Corsico, A., Giampietro, V., Lawrence, N., Deeley, Q., Murphy, D.G.M., Kucharska-Pietura, K., et al., 2008. Genetic variation in the serotonin transporter modulates neural system-wide response to fearful faces. Genes Brain Behav. 7 (5), 543–551.

Tashiro, M., Itoh, M., Fujimoto, T., Fujiwara, T., Ota, H., Kubota, K., Higuchi, M., Okamura, N., Ishii, K., Bereczki, D., et al., 2001. 18F-FDG PET mapping of regional brain activity in runners. J. Sports Med. Phys. Fitness 41 (1), 11–17.

Thomson, A.M., Bannister, A.P., 1998. Postsynaptic pyramidal target selection by descending layer III pyramidal axons: dual intracellular recordings and biocytin filling in slices of rat neocortex. Neuroscience 84 (3), 669–683.

Uphouse, L., Montanez, S., Richards-Hill, R., Caldarola-Pastuszka, M., Droge, M., 1991. Effects of the 5-Ht1a agonist, 8-oh-dpat, on sexual behaviors of the proestrous rat. Pharmacol. Biochem. Behav. 39 (3), 635–640.

Uphouse, L., Caldarolapastuszka, M., Montanez, S., 1992. Intracerebral actions of the 5-HT1a agonists, 8-oh-dpat and buspirone and of the 5-Ht1a partial agonist antagonist, nan-190, on female sexual-behavior. Neuropharmacology 31 (10), 969–981.

van Wingen, G., Mattern, C., Verkes, R.J., Buitelaar, J., Fernandez, G., 2008. Testosterone biases automaticmemory processes in women towards potentialmates. Neuroimage 43 (1), 114–120.

Watakabe, A., Komatsu, Y., Sadakane, O., Shimegi, S., Takahata, T., Higo, N., Tochitani, S., Hashikawa, T., Naito, T., Osaki, H., et al., 2009. Enriched expression of serotonin 1B and 2A receptor genes in macaque visual cortex and their bidirectional modulatory effects on neuronal responses. Cereb. Cortex 19 (8), 1915–1928.

Worsley, K.J., Marrett, S., Neelin, P., Vandal, A.C., Friston, K.J., Evans, A.C., 1996. A unified statistical approach for determining significant signals in images of cerebral activation. Hum. Brain Mapp. 4 (1), 58–73.

Yamamori, T., 2011. Selective gene expression in regions of primate neocortex: implications for cortical specialization. Prog. Neurobiol. 94 (3), 201–222.

SUPPORTING INFORMATION

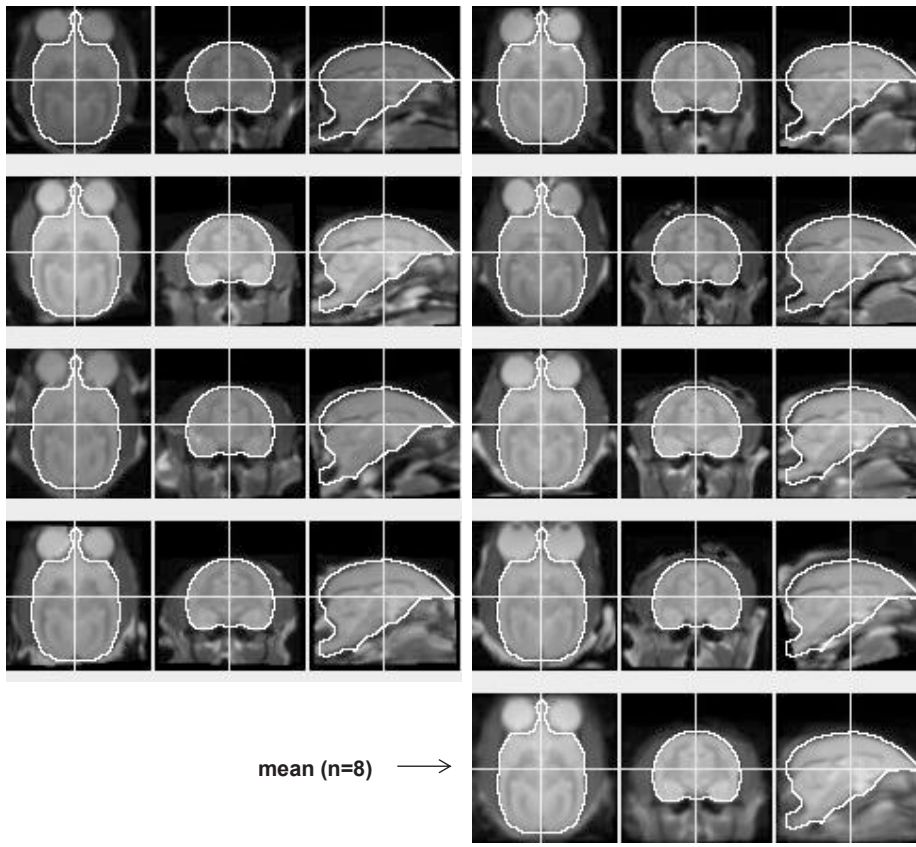

Supplementary Figure 1. Alignment of individual MRIs. The first eight images show axial, coronal, and sagittal slices in each subject's aligned MRI at the same position. Individual images have been aligned to the target (cj1074) by 6 degrees of freedom (rigid body) and then by 9 degrees of freedom (rigid body plus zooms). The last image shows the mean image, used as the MRI template. The whole brain contour is the same in all views and demonstrates the quality of the alignments.

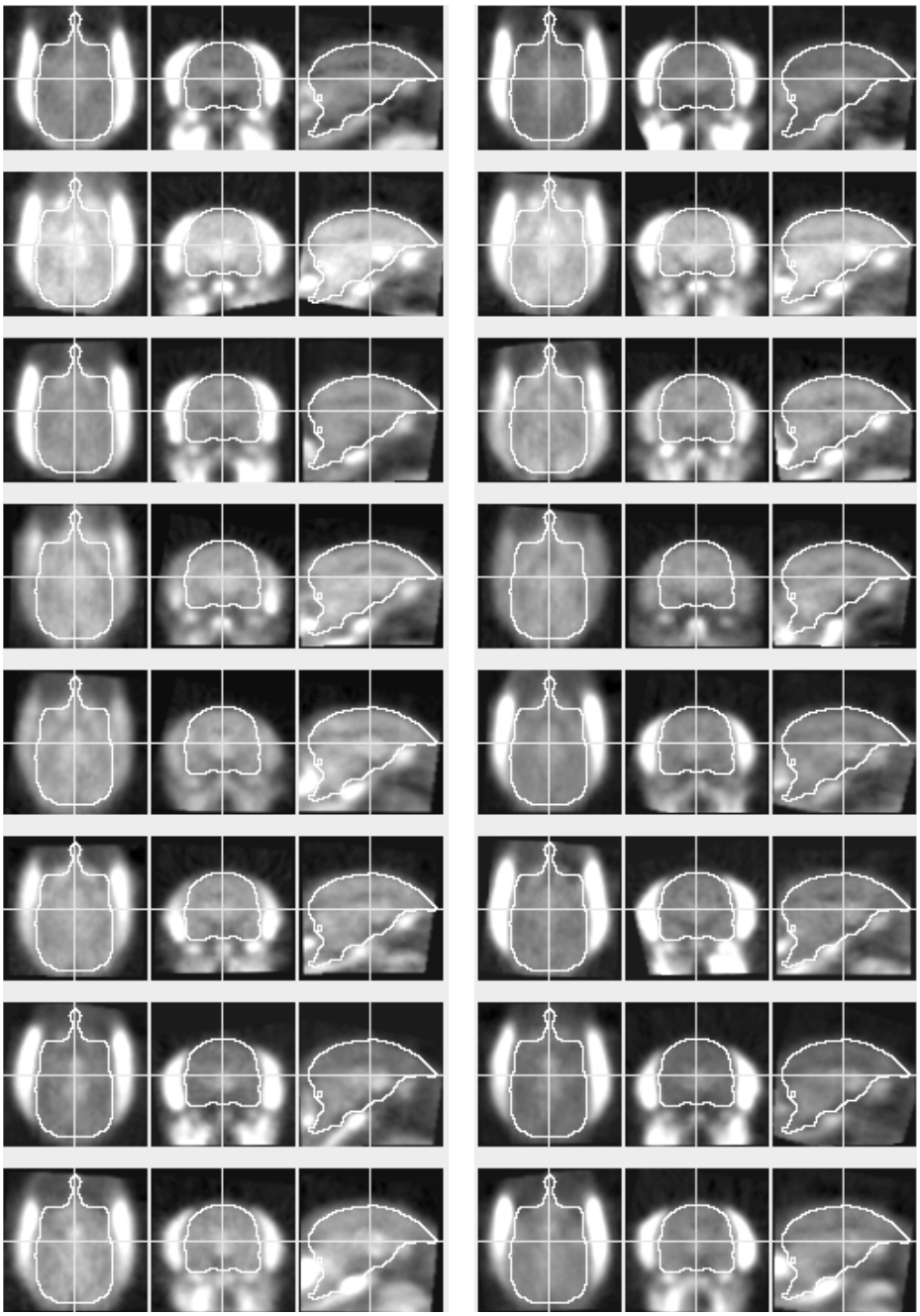

Supplementary Figure 2. Individual FDG images. Each row shows axial, coronal, and sagittal slices of FDG image for one subject in Saline condition (left) and DPAT condition (right). Contour is on whole brain mask modified to avoid contributions from FDG uptake outside of brain.

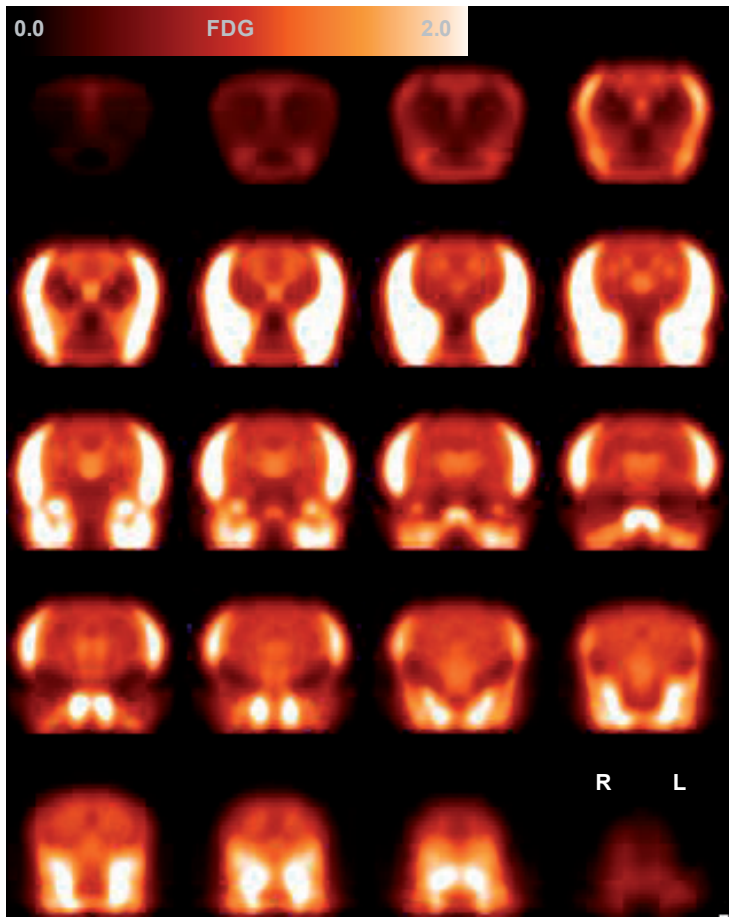

Supplementary Figure 3. Mean FDG Image. Average of 16 (8 subjects x 2 conditions) whole brain normalized images. Every fourth 0.5 mm slice shown.

Supplementary Figure 4. No ROI shows a significant response to chronic 8-OH-DPAT treatment. Mean whole brain normalized radioactivity in each condition (Saline, 8-OH-DPAT) for each ROI and all subjects ($p>0.3$ for each region; paired t test, 2-tailed; n = 8).

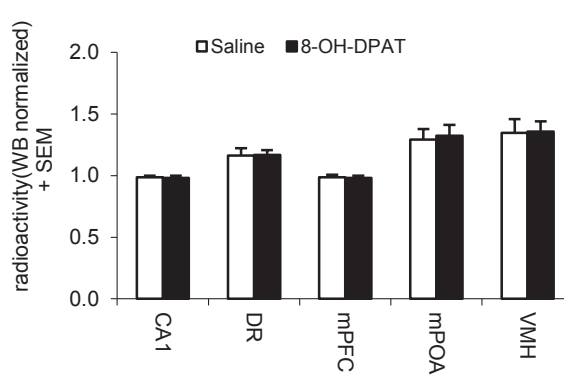

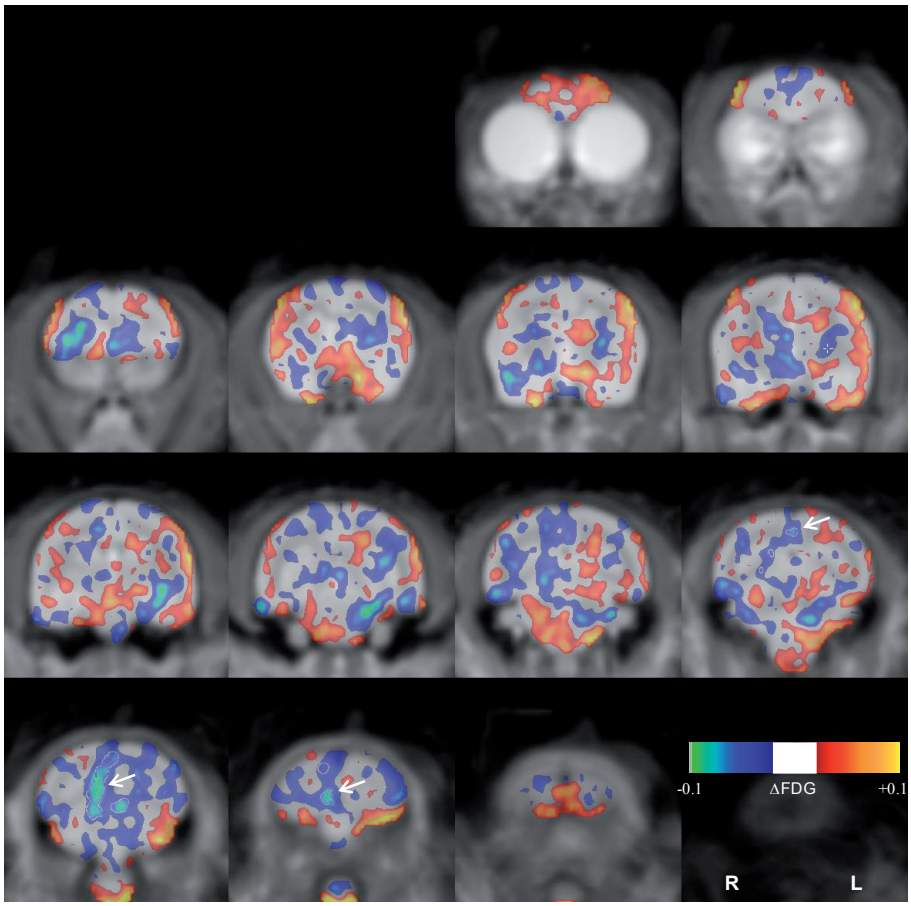

Supplementary Figure 5. Glucose metabolism index decreases in medial occipital cortex in response to chronic 8-OH-DPAT treatment. The color scale indicates the mean difference in whole brain normalized radioactivity, ΔFDG = 8-OH-DPAT minus Saline, thresholded at $0.02 < |\Delta FDG| < 0.10$. The white contour marked by arrows delineates a significant negative cluster (2-tailed paired t test, $p_{uncorrected} < 0.05$, extent = 60 μL, $p_{corrected} = 0.004$). Every fourth 0.62 mm coronal slice shown.

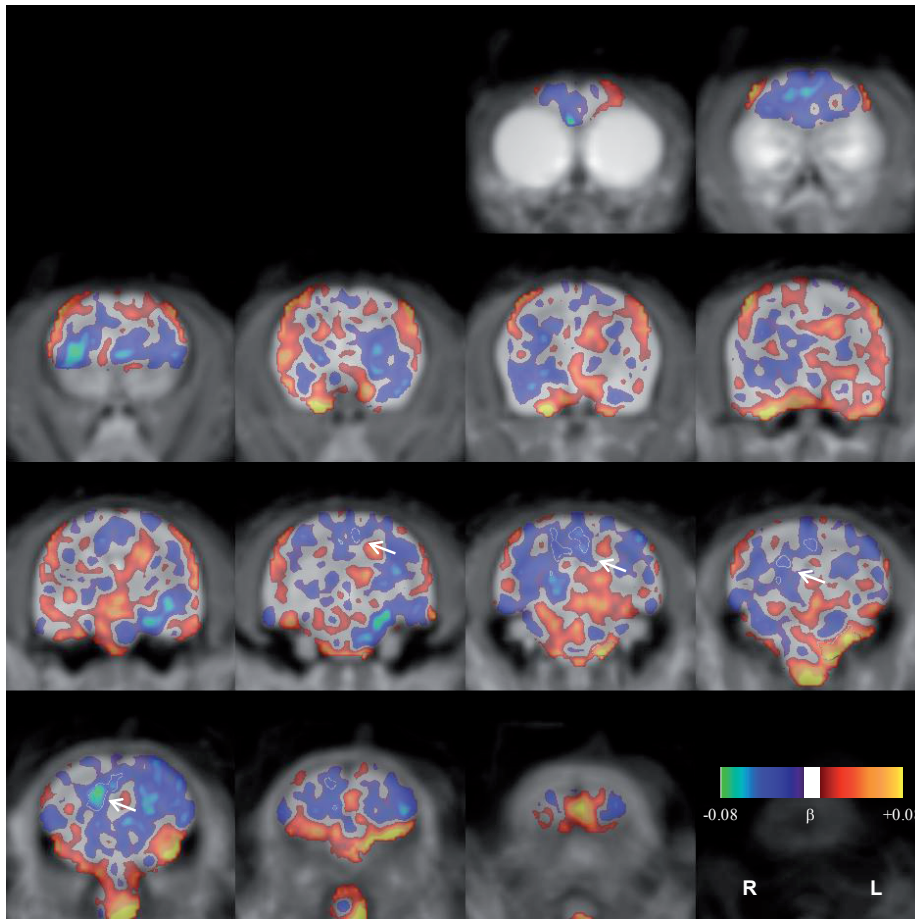

Supplementary Figure 6. Changes in glucose metabolism index correlate with alterations in female rejection of mounts. Between-condition difference in normalized FDG uptake (8-OH-DPAT minus Saline) correlated against alteration in behavior. Color scale corresponds to slope of linear correlation through the origin, $\Delta FDG = \beta * \Delta(\text{Reject Mount})$, thresholded at $0.01 < |\beta| < 0.08$. For Pearson r, 2-tailed $p_{uncorrected} < 0.05$, two significant clusters were identified, one with a positive correlation (left ventral cerebellum; extent = 47 µL; $p_{corrected} = 0.017$) and one with a negative correlation (medial occipital cortex; extent = 72 µL; $p_{corrected} = 0.001$; indicated by arrows). Every fourth 0.62 mm coronal slice shown.

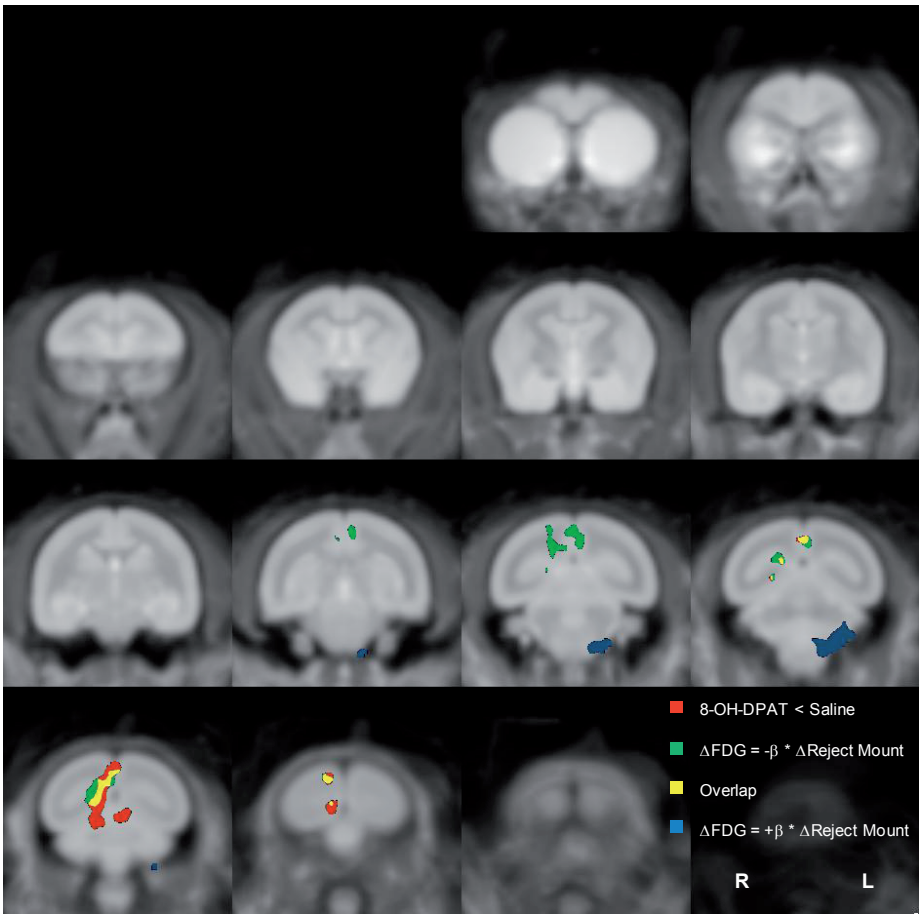

Supplementary Figure 7. Overlap between contrast and correlation clusters shown in Supplementary Figures 5 and 6. Cluster of voxels with significant reduction in FDG radioactivity during 8-OH-DPAT condition compared to Saline condition (**red**; paired t test, 2-tailed $p_{uncorrected} < 0.05$, extent 60 µL, $p_{corrected} = 0.004$). Cluster of voxels with significant negative correlation between alterations of FDG radioactivity and rejection of mount attempts between conditions (**green**; Pearson r; 2-tailed $p_{uncorrected} < 0.05$, extent 72 µL, $p_{corrected} = 0.001$). The two clusters overlap (**yellow**; 23 µL). Significant cluster with positive correlation is seen as well in left ventral cerebellum (**blue**; Pearson r; 2-tailed $p_{uncorrected} < 0.05$, extent 47 µL, $p_{corrected} = 0.017$). Every fourth 0.62 mm coronal slice shown. This image shown in orthogonal views in **Fig. 7**.

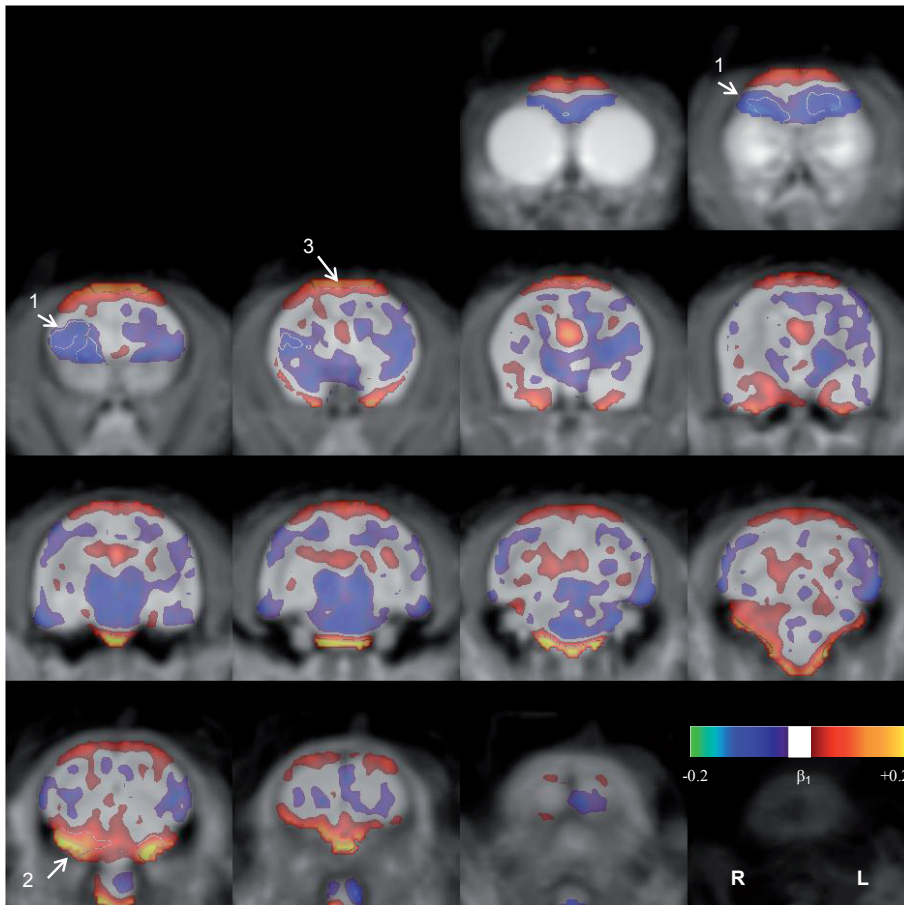

Supplementary Figure 8. Glucose metabolism index correlated against female rejection of mounts in Saline condition. Three significant clusters indicated by numbers and arrows. Negative correlation (blue), i.e. less rejection of mounts with increasing FDG uptake: (1) bilateral orbitofrontal cortex and right insular cortex (Pearson r; 2-tailed puncorrected < 0.05, extent 122 μL, pcorrected = 0.000). Positive correlation (red): (2) bilateral ventral cerebellum (161 μL, pcorrected = 0.000) and (3) bilateral dorsal frontal cortex (115 μL, pcorrected = 0.001). FDG = β_1 * Reject Mount + β_2. Arbitrarily thresholded at 0.02 < |β_1| < 0.2. Every fourth 0.62 mm coronal slice shown.